Nanoscale

Accepted Manuscript

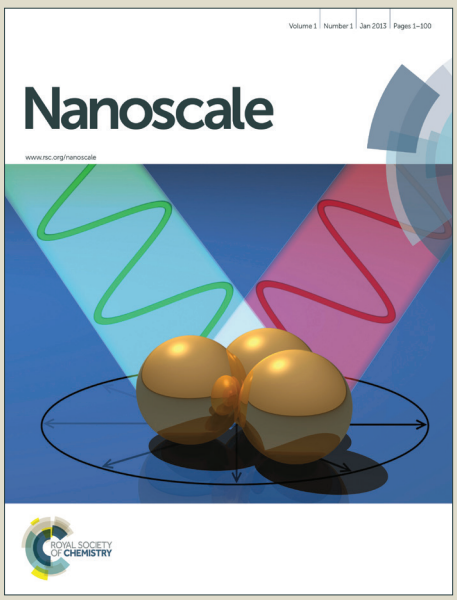

ROYAL SOCIETY OF CHEMISTRY

www.rsc.org/nanoscale

Journal Name

RSCPublishing

COMMUNICATION

High Efficient Hybrid Solar Cells with Tunable Dipole at the Donor/Acceptor Interface

Cite this: DOI: 10.1039/x0xx00000x

Weifei Fu,[a,‡] Ling Wang,[a,‡] Jun Ling,[a] Hanying Li,[a] Minmin Shi,[a,*] Jiangeng Xue,[b,*] Hongzheng Chen[a,*]

Received 00th January 2012,
Accepted 00th January 2012

DOI: 10.1039/x0xx00000x

www.rsc.org/

Effects of molecular dipole at the conjugated polymer/nanocrystal interface on the energy level alignment, exciton dissociation process, and consequently the photovoltaic performance of poly[2,6-(4,4-bis-(2-ethylhexyl)-4H-cyclopenta[2,1-b;3,4-b']-dithiophene)-alt-4,7-(2,1,3-benzothiadiazole)] (PCPDTBT):CdSe quantum dots bulk heterojunction hybrid solar cells are systemically studied. Power conversion efficiency up to 4.0% is achieved when 4-fluorobenzenethiol is used for ligand exchange.

Since Alivisatos *et al.* demonstrated the first conjugated polymer/nanocrystal solar cells based on poly(3-hexylthiophene) (P3HT) and cadmium selenide (CdSe) nanocrystals in 2002,[1] hybrid solar cells (HSCs) have attracted much attention due to the potentially high electron mobility and tunable band gap of nanocrystals.[2-7] The power conversion efficiencies (PCEs) of HSCs have been increasing continuously these years with advances in material synthesis and processing as well as device architectures.[4, 8-10] CdSe nanocrystals are the most investigated traditional nanocrystals for HSCs due to their mature synthetic process and easy shape control.[5] PCE of 1.9% was obtained after increasing the size of CdSe quantum dots (QDs) and further improved to 2.4% with a layer of ZnO nanoparticles acting as cathode buffer for P3HT:CdSe QDs HSCs.[11, 12] Recently it has reached a value of up to 3.09% through post-deposition ligand exchange by n-butanethiol (nBT) in our laboratory.[13] When a lower band-gap polymer, poly[2,6-(4,4-bis-(2-ethylhexyl)-4H-cyclopenta[2,1-b;3,4-b']-dithiophene)-alt-4,7-(2,1,3-benzothiadiazole)] (PCPDTBT) was used instead of P3HT as donor to extend the spectral sensitivity of the HSCs into the near-infrared region, a maximum PCE of 3.7% was obtained.[14] This improvement is also attributed to electronic and optical effect of the additional ZnO nanoparticle based cathode buffer layer, which improves the light harvesting and reduces surface recombination. Furthermore, when nanorods, which have perceived advantages in supporting directional charge transport paths for efficient charge transport, was employed as the acceptor material togethner with proper interface modification, a maximum PCE of 4.7±0.3% was achieved.[15] Last but not least, compared to the widely used cadmium chalcogenide nanocrystals, lead chalcogenides emerged as another promising materials for HSCs with advantages of higher bandgap tunablity and charge mobility.[8, 16, 17] Very recently a record HSCs efficiency of 5.5% was obtained by Ma *et al.* with judicious device optimization based on poly(2,6-(N-(1-octylnonyl) dithieno[3,2-b:20,30-d]pyrrole)-alt-4,7-(2,1,3-benzothiadiazole)) (PDTPBT)/PbS_xSe_{1-x} nanocrystals.[8]

However, such efficiency values significantly lag behind that of all-organic solar cells with fullerenes and their derivatives such as [6,6]-phenyl-$C_{61/71}$-butyric acid methyl ester ($PC_{61/71}BM$) as electron acceptor, in which efficiency of 10% has been reported recently.[18-21] The critical challenge for achieving superior device performance of HSCs lies in the complex surface of nanocrystals when compared to that of fullerene derivatives in all-organic solar cells.[5] Following their synthesis in solution, nanocrystals are generally capped by long-chain organic ligands (such as oleic acid (OA)) to ensure their solution processability. These insulating barriers between nanocrystals or between polymers and nanocrystals prevent efficient charge transfer and carrier transport in solid-state films, thus hindering photon-to-electron conversion and resulting in low quantum efficiencies.[5, 22, 23, 24] Much attention has therefore been devoted to develop efficient ligands that minimize the interparticle spacing to promote charge transfer between polymer and nanocrystals and carrier transport in the film.[1, 15] Short chain alkylthiols and aromatic thiols are the main ligands widely used now and show promising in effective surface passivation while reducing interparticle spacing to achieve high efficiencies for HSCs.[8, 15, 25, 26] According to the protocols developed to examine interface dipole effects induced by self-assembled monolayers on Au,[27, 28] Ag,[28] and indium-tin oxide (ITO) surfaces,[29-32] the organic capping ligands may alter the surface electronic structures of nanocrystals, which has

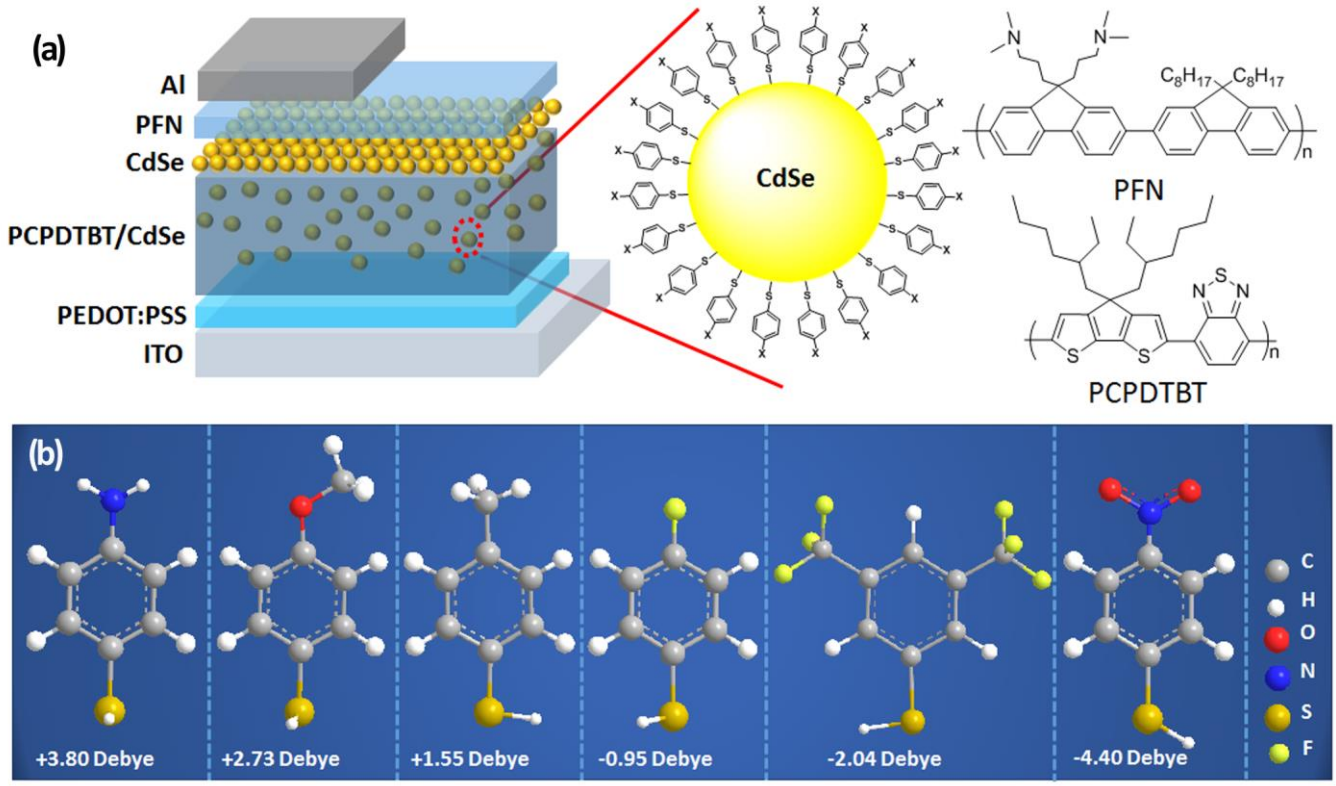

Figure 1. (a) Schematic hybrid solar cell device structure used in this study. The surface chemistry of CdSe QDs after ligand exchange with benzenethiol and chemical structures of PFN and PCPDTBT are also shown here. (b) Chemical structures of six benzenethiols with different dipoles (BT-NH_2, BT-OCH_3, BT-CH_3, BT-F, BT-$(CF_3)_2$, BT-NO_2) used in this study.

been demonstrated for InAs[33] and CdSe[34] QDs. However, little is known on how the ligands affect the electronic structure, exciton dissociation process at the polymer/nanocrystal interface and sequentially the photovoltaic performance.[35, 36] In this work, these interfacial properties were systematically investigated with different molecular dipoles at PCPDTBT/CdSe QDs interface. HSCs with modified donor/acceptor (D/A) interface were also fabricated to establish the relationship between the photovoltaic performance and D/A interface. After fine tuning the D/A interface, a high PCE of 4.0% was obtained for our HSCs. To our knowledge, this is among the highest PCE ever reported for CdSe QD based HSCs.

HSCs were fabricated with the device structure of ITO/ poly(3,4-ethylenedioxylenethiophene):poly(4-styrene sulfonic acid) (PEDOT:PSS) /PCPDTBT:CdSe QDs/ poly [(9,9-bis(3′-(*N*,*N*-dimethylamino) propyl)-2,7-fluorene)-*alt*-2,7-(9,9–dioctylfluorene)] (PFN)/Al shown in **Figure 1**a. Six benzenethiols (BTs) with different substituents (-NH_2, -OCH_3, -CH_3, -F, -$(CF_3)_2$, -NO_2) are chosen to modify the interface between PCPDTBT and CdSe QDs, which are employed as the electron donor and acceptor, respectively. CdSe QDs were used as electron acceptors in our work due to the easily synthesis procedure comparing to the nanorods and tetrapods. The chemical structures and the calculated molecular dipoles of the benzenethiols (BT-NH_2, BT-OCH_3, BT-CH_3, BT-F, BT-$(CF_3)_2$, BT-NO_2) are shown in Figure 1b. The molecular dipole moments, which range from +3.80 D (BT-NH_2) to –4.40 D (BT-NO_2), were obtained after geometry optimization carried out by the density functional theory (DFT) calculation at the B3LYP/6-31G (d) level, using the Gaussian 03 program.[37] Figure 1a also shows the surface chemistry of CdSe QDs after ligand exchange with benzenethiols. It is demonstrated that thiols have strong affinity with Cd^{2+} on the surface of CdSe QDs, and are believed to replace the X-type (charged) ligands by forming Cd-thiolates.[15] Hence, during a post-deposition ligand exchange process, benzenethiols could potentially form a self-assembled monolayer at the D/A interface,[38, 39] replacing the original long chain ligands. This was demonstrated by the Fourier transform infrared spectra shown in Figure S1.

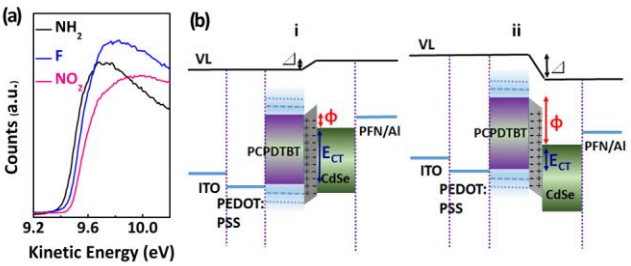

Figure 2. (a) Typical UPS spectra of CdSe QDs films modified by benzenethiols with different dipole. (b) Schematic illustration of the energy level diagram of the devices with different molecular dipoles at the D/A interface. (i) For BT-CH_3, BT-OCH_3, BT-NH_2, positive molecular dipoles (pointing into QDs) shift QD energy levels up, such that excitons cannot efficiently be dissociated with a small driving force (φ). (ii) For BT-F, BT-$(CF_3)_2$, BT-NO_2, negative dipoles shift the QD energy levels down, thus excitons excited at lower photon energies can be efficiently dissociated with a large driving force.

Figure 2a shows the typical ultraviolet photoemission spectroscopic (UPS) spectra of the CdSe QDs after modification by benzenethiols with different dipoles. Clearly, we can found that the molecular dipole of the ligands on nanocrystal surface affects the work function (WF) of the CdSe QDs, which is a linear increasing

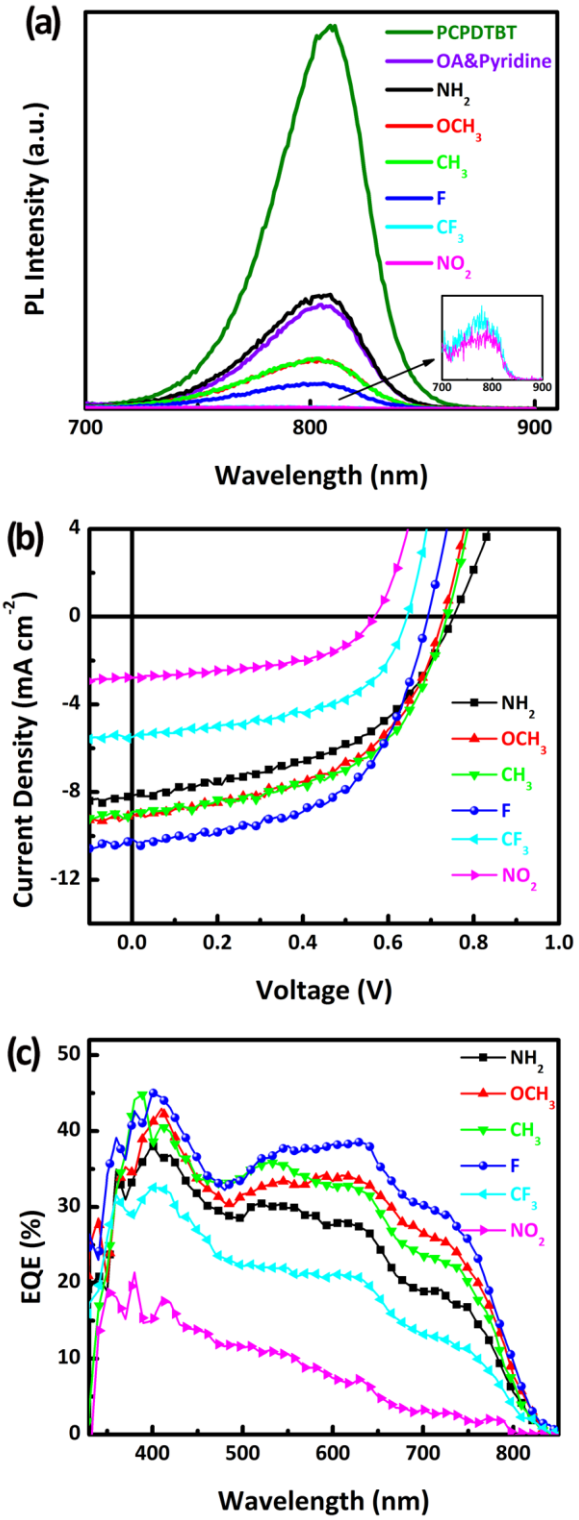

Figure 3. (a) PL spectra of the pristine PCPDTBT film and PCPDTBT/CdSe QDs blend films with different dipoles at the D/A interface. (b) J-V characteristics of HSC devices with different molecular dipoles at the polymer/CdSe QDs interface under simulated 1 sun AM 1.5 solar illumination. (c) EQE of the devices with different molecular dipoles at the D/A interface.

function of the kinetic energy corresponding to the photoemission onset (or secondary electron cut-off). Decreasing the dipole moment of the benzenethiols from positive to negative results in an increaseof the WF in the order of BT-NH_2 (+3.80 D) < BT-F (-0.95 D) < BT-NO_2 (-4.40 D), by an overall amount of 70 meV. The schematic illustration of the energy level diagram of our devices is shown in Figure 2b (i, ii). The driving force (φ) is defined as the difference between the energy of the excited polymer singlet exciton (E_{D^*A}) and the energy of the charge transfer (CT) states (E_{CT}).[40] We see that the driving force increases due to the increased WF of the QDs when decreasing the dipole moment from positive to negative. Larger driving force has been demonstrated to be beneficial for the dissociation of CT states into separated electrons and holes.[40, 41]

Steady-state photoluminescence (PL) measurements were conducted to study the exciton dissociation process with different dipoles at the D/A interface. As shown in **Figure 3**a, PCPDTBT/CdSe QDs films containing QDs modified with different benzenethiols show various levels of PL quenching compared to the neat polymer film. Stronger PL quenching was observed with decreasing the BT molecular dipole. Particularly, the PCPDTBT PL is entirely quenched when the CdSe QDs contain the most negative dipoles (BT-$(CF_3)_2$ and BT-NO_2). Since the absorption and morphology of the hybrid films remain the same after post-deposition ligand exchange (see Figure S2 and S3 in Supporting Information, as well as in our previous work[13]), the increased level of polymer PL quenching could be attributed to the larger driving force obtained by decreasing the dipole moment at D/A interface facilitating the exciton dissociation process, which is a prerequisite for achieving high efficient photovoltaic devices,[42] or to the creation of localized states at the interface causing excitons in polymers to recombine non-radiatively.[43, 44] As will be shown later, the latter may be the case for BT-$(CF_3)_2$ and BT-NO_2 when the very negative dipoles result in localized recombination centers at the QD surface.

Figure 3b shows the current density (*J*)-voltage (*V*) characteristics of HSCs with different molecular dipoles at the D/A interface under simulated 1 sun AM 1.5 solar illumination. The photovoltaic performance parameters are also summarized in **Table 1**. We can see that the PCE of devices improves with decreasing the dipole moment at the D/A interface in the order of BT-NH_2, BT-OCH_3, BT-CH_3, BT-F, with main contributions from the improvement in the short-circuit current density (J_{sc}) and fill factor (FF). However, further decreasing the dipole moment to even stronger negative dipoles (BT-$(CF_3)_2$, BT-NO_2) leads to significant reduction in J_{sc} and therefore PCE. It could be that the most negative dipoles create localized states causing polymer excitons to recombine non-radiatively. The best performance of devices, with BT-F at the D/A interface, is obtained by a compromise between the effects of molecular dipole on the exciton dissociation and recombination. On the other hand, our results show that the V_{oc} is highly dependent on E_{CT}, which agrees well with the widely accepted theory.[40] Devices modified by BT-NH_2, BT-OCH_3, BT-CH_3 own a similar V_{oc} of 0.73-0.75 V with higher E_{CT}, while devices modified by BT-F show slightly lower V_{oc} of 0.68±0.01 V, and BT-NO_2 modified devices show the lowest V_{oc} of 0.58±0.01 V due to the lowest E_{CT}. The change in V_{oc} qualitatively agrees with the change in the WF of the modified QDs from the UPS measurements. Overall, the devices modified with BT-F show a highest PCE of 3.99%, with J_{sc} of 10.17 mA cm^{-2}, V_{oc} of 0.69 V, and FF of 0.570. This improved performance is believed due to the larger driving force induced by the appropriate molecular dipole at the D/A interface besides the enhanced electronic coupling between PCPDTBT and CdSe QDs after removal of the long chain surfactants.

The EQE of the devices with different interface dipoles are compared in Figure 3c. As a similar trend as J_{sc}, EQE was gradually improved in the order of devices involving self-assembled monolayer of BT-NH_2, BT-OCH_3, BT-CH_3, BT-F, mainly in the

Table 1. Summary of photovoltaic performance of PCPDTBT:CdSe QD HSCs with different molecular dipoles at the D/A interface, which represent statistical averages of over 20 devices for each configuration.

Ligand	Dipole [Debye]	WF of CdSe QDs [eV]	V_{OC} [V]	J_{SC} [mA cm^{-2}]	FF [%]	PCE [%]
OA/Pyridine	/	/	0.77 ±0.01	4.47 ±0.19	42.8 ±1.7	1.46 ±0.11
BT-NH_2	+3.80	4.61	0.75 ±0.01	7.92 ±0.21	47.6 ±2.1	2.82 ±0.18
BT-OCH_3	+2.73	4.61	0.73 ±0.01	8.99 ±0.30	51.2 ±1.1	3.36 ±0.06
BT-CH_3	+1.55	4.61	0.73 ±0.01	8.88 ±0.36	52.5 ±1.6	3.41 ±0.19
BT-F	-0.95	4.65	0.68 ±0.01	9.93 ±0.28	57.7 ±1.3	3.91 ±0.07
BT-$(CF_3)_2$	-2.04	4.65	0.63 ±0.01	5.30 ±0.23	53.6 ±0.5	1.80 ±0.09
BT-NO_2	-4.40	4.68	0.58 ±0.01	2.77 ±0.06	47.6 ±2.7	0.76 ±0.05

long wavelength range between 500-850 nm, which corresponds to the absorption by the polymer. This agrees with our explanation above that the higher driving force obtained with negative dipoles at the D/A interface improves the separation of charges in excitons generated from the polymer. A maximum EQE value of 38.6% was obtained for BT-F modified devices at 625 nm, which is much higher than the previously reported 30% at the same wavelength.[45, 46] These results indicate that the molecular dipole between polymer and nanocrystals significantly affects the photon-to-electron conversion, which has not been fully investigated before. Although there is only 10% PCPDTBT in weight or ~30% in volume in the active layer of HSCs, the low band gap polymer contributes strongly to the light absorption due to its high absorption coefficient and its ability to harvest the near-infrared photons. Choosing ligands with appropriate dipole moment is critical for efficiently converting the long wavelength photons to electrons to achieve higher photocurrent.

Conclusions

In conclusion, the effects of molecular dipoles between PCPDTBT and CdSe QDs on the energy level alignment, exciton dissociation process, and consequently the photovoltaic performance were systematically investigated. Decreasing the dipole moment from positive to negative can increase the driving force thus facilating exciton dissociation at the D/A interface. However, the very negative molecular dipoles may create localized states causing polymer excitons to recombine non-radiatively. High performance hybrid solar cells based on PCPDTBT:CdSe QDs are demonstrated with a highest efficiency of 4.0% when 4-fluorobenzenethiol is used for ligand exchange. While we have only focused on CdSe QDs in this work, our results show that judicious choice of ligands with appropriate molecular dipoles have a strong impact on the polymer/nanocrystal interface chemical and electronic structures and subsequently on photovoltaic device performance. This research could open up a new pathway to further improving the performance of BHJ HSCs that involve more efficient nanostructures (e.g. nanorods) and/or more advanced designs of conjugated polymers.

Experimenatal Section

CdSe QDs synthesis: CdSe QDs were synthesized according to the reported procedure.[12] In a typical synthetic process, CdO (76 mg), trioctylphosphine oxide (TOPO, 3.0 g) and oleic acid (OA, 3.0 ml) were added into the reactor and the mixture was heated to 285 °C under vigorous stirring in nitrogen atmosphere. Se (80 mg) was added into trioctylphosphine (TOP, 1.0 ml) and the mixture was sonicated until the solution became clear. The Se-TOP solution was then quickly injected into the reactor. 5 min later, the hot solution was quickly transferred into toluene (5 ml). The as-prepared CdSe QDs were washed with methanol and centrifuged twice, then dispersed in pyridine (15 ml) and stirred for 24 h. The resulting nanocrystals were flocculated by hexane and centrifuged.

Device fabrication and testing: Prior to fabrication, the substrates were cleaned by sonication using detergent, deionized water, acetone, and isopropanol sequentially for every 15 min followed by 15 min of ultraviolet ozone (UV-Ozone) treatment. Then a layer of PEDOT: PSS (Baytron P AI4083) was spin-coated onto the cleaned ITO and baked in air at 140 °C for 15 min. The substrates were transferred to a glovebox for spin coating of PCPDTBT:CdSe QDs (1:9, w/w, chlorobenzene/pyridine (9:1), 35 mg/ml) active layer with the thickness of about 90 nm. The post-deposition ligand-exchange process was carried out by soaking the as-prepared films in a solution of 0.01 M benzenethiol in acetonitrile for 30 s, then rinsed with pure acetonitrile twice to remove the excess of benzenethiol and OA. Subsequently, a thin pure nanocrystal layer was deposited onto the blend film from a 5 mg mL^{-1} CdSe QDs solution in hexane, then ligand exchanged and cleaned as above. Then 5 nm thick PFN film was deposited on as cathode buffer layer by spin-coating from 0.4 mg/ml PFN in methanol. Subsequently, samples were loaded into a vacuum deposition chamber (background pressure ≈ 5×10^{-4} Pa) to deposit a 100 nm thick Al cathode with a shadow mask defining an active device area of 5.2 mm^2. The *J-V* characteristics were measured with Keithley 2400 measurement source units with the devices maintained at room temperature in air. The photovoltaic response was measured under a calibrated solar simulator (Abet 300 W) at 100 mW cm^{-2}, and the light intensity was calibrated with a standard photovoltaic reference cell. The EQE spectrum was measured using a Stanford Research System Model SR830 Lock-in Amplifier unit coupled with a monochromator and a 500W xenon lamp, and a calibrated Si photodiode with known spectral response was used as a reference.

Material characterization: The UPS measurements were carried out in an integrated ultrahigh vacuum system equipped with multi-

technique surface analysis system (Thermo ESCALAB 250Xi) with the He (I) (21.2 eV) UV excitation source. A negative bias voltage of -4.8V was applied to the samples in order to shift the spectra from the spectrometer threshold. The steady-state PL spectra were taken on a FluoroMax-4 HORIBA Jobin Yvon spectrofluorometer. The hybrid films were prepared on the silicon substrate with thickness of about 90 nm and treated with different benzenethiols under the same conditions as film preparation method for devices. The thickness of PCPDTBT film is about 50 nm. The excitation light of 620 nm enters the sample side with light power of 500 mW, and the PL emission is collected from the sample side in the range of 700-900 nm.

Acknowledgment

This work was supported by the Major State Basic Research Development Program (2014CB643503) and the National Natural Science Foundation of China (Grants 91233114, 51261130582, and 50990063).

Notes and references

[a]State Key Laboratory of Silicon Materials, MOE Key Laboratory of Macromolecular Synthesis and Functionalization, Department of Polymer Science and Engineering, Zhejiang University, Hangzhou 310027, P. R. China. *Address correspondence to hzchen@zju.edu.cn

[b]Department of Materials Science and Engineering, University of Florida, Gainesville, Florida 32611-6400, United States.

†Electronic Supplementary Information (ESI) available: FTIR spectra of CdSe QD films with various ligands; Absorption spectra and atomic force microscope (AFM) images of PCPDTBT:CdSe QDs hybrid films treated by different benzenethiols. See DOI: 10.1039/c000000x/

‡These authors contributed equally.

1. Huynh, W. U.; Dittmer, J. J.; Alivisatos, A. P. *Science*, 2002, **295**, 2425-2427.
2. L. Roiban, L. Hartmann, A. Fiore, D. Djurado, F. Chandezon, P. Reiss, J. F. Legrand, S. Doyle, M. Brinkmann and O. Ersen, *Nanoscale*, 2012, **4**, 7212-7220.
3. M. Lopez-Haro, T. Jiu, P. Bayle-Guillemaud, P.-H. Jouneau and F. Chandezon, *Nanoscale*, 2013, **5**, 10945-10955.
4. Greaney, M. J.; Araujo, J.; Burkhart, B.; Thompson, B. C.; Brutchey, R. L. *Chem. Commun.*, 2013, **49**, 8602-8604.
5. Zhou, R.; Xue, J. *Chemphyschem* 2012, **13**, 2471-80.
6. Zhou, Y.; Eck, M.; Kruger, M. *Energy Environ. Sci.*, 2010, **3**, 1851-1864.
7. Moule, A. J.; Chang, L.; Thambidurai, C.; Vidu, R.; Stroeve, P. *J. Mater. Chem.*, 2012, **22**, 2351-2368.
8. Liu, Z.; Sun, Y.; Yuan, J.; Wei, H.; Huang, X.; Han, L.; Wang, W.; Wang, H.; Ma, W. *Adv. Mater.*, 2013, **25**, 5772-5778.
9. Chen, Z.; Zhang, H.; Yu, W.; Li, Z.; Hou, J.; Wei, H.; Yang, B. *Adv. Energy Mater.*, 2012, **3**, 433-437.
10. Chen, Z.; Zhang, H.; Du, X.; Cheng, X.; Chen, X.; Jiang, Y.; Yang, B. *Energy Environ. Sci.*, 2013, **6**, 1597-1603.
11. Yang, J.; Tang, A.; Zhou, R.; Xue, J. *Sol. Energy Mater. Sol. Cells*, 2011, **95**, 476-482.
12. Qian, L.; Yang, J.; Zhou, R.; Tang, A.; Zheng, Y.; Tseng, T.-K.; Bera, D.; Xue, J.; Holloway, P. H. *J. Mater. Chem.*, 2011, **21**, 3814-3817.
13. Fu, W.; Shi, Y.; Qiu, W.; Wang, L.; Nan, Y.; Shi, M.; Li, H.; Chen, H. *Phys. Chem. Chem. Phys.*, 2012, **14**, 12094-12098.
14. Zhou, R.; Zheng, Y.; Qian, L.; Yang, Y.; Holloway, P. H.; Xue, J. *Nanoscale*, 2012, **4**, 3507-14.
15. Zhou, R.; Stalder, R.; Xie, D.; Cao, W.; Zheng, Y.; Yang, Y.; Plaisant, M.; Holloway, P. H.; Schanze, K. S.; Reynolds, J. R.; Xue, J. *ACS Nano*, 2013, **7**, 4846-4854.
16. Nam, M.; Park, J.; Kim, S.-W.; Lee, K. *J. Mater. Chem. A*, 2014, **2**, 3978-3985.
17. Seo, J.; Cho, M. J.; Lee, D.; Cartwright, A. N.; Prasad, P. N. *Adv. Mater.*, 2011, **23**, 3984-3988.
18. You, J.; Dou, L.; Yoshimura, K.; Kato, T.; Ohya, K.; Moriarty, T.; Emery, K.; Chen, C.-C.; Gao, J.; Li, G.; Yang, Y. *Nat. Commun.*, 2013, **4**, 1446.
19. You, J.; Chen, C.-C.; Hong, Z.; Yoshimura, K.; Ohya, K.; Xu, R.; Ye, S.; Gao, J.; Li, G.; Yang, Y. *Adv. Mater.*, 2013, **25**, 3973-3978.
20. He, Z.; Zhong, C.; Su, S.; Xu, M.; Wu, H.; Cao, Y. *Nat. Photon.*, 2012, **6**, 593-597.
21. Guo, X.; Cui, C.; Zhang, M.; Huo, L.; Huang, Y.; Hou, J.; Li, Y. *Energy Environ. Sci.*, 2012, **5**, 7943-7949.
22. Tang, J.; Kemp, K. W.; Hoogland, S.; Jeong, K. S.; Liu, H.; Levina, L.; Furukawa, M.; Wang, X.; Debnath, R.; Cha, D.; Chou, K. W.; Fischer, A.; Amassian, A.; Asbury, J. B.; Sargent, E. H. *Nat. Mater.*, 2011, **10**, 765-771.
23. Fu, W.-F.; Shi, Y.; Wang, L.; Shi, M.-M.; Li, H.-Y.; Chen, H.-Z. *Sol. Energy Mater. Sol. Cells*, 2013, **117**, 329-335.
24. M. Ramanathan, L. K. Shrestha, T. Mori, Q. Ji, J. P. Hill and K. Ariga, *Phys. Chem. Chem. Phys*., 2013, **15**, 10580-10611.
25. Greaney, M. J.; Das, S.; Webber, D. H.; Bradforth, S. E.; Brutchey, R. L. *ACS Nano*, 2012, **6**, 4222-4230.
26. Chen, H.-C.; Lai, C.-W.; Wu, I. C.; Pan, H.-R.; Chen, I. W. P.; Peng, Y.-K.; Liu, C.-L.; Chen, C.-h.; Chou, P.-T. *Adv. Mater.*, 2011, **23**, 5451-5455.
27. Alloway, D. M.; Hofmann, M.; Smith, D. L.; Gruhn, N. E.; Graham, A. L.; Colorado, R.; Wysocki, V. H.; Lee, T. R.; Lee, P. A.; Armstrong, N. R. *J. Phys. Chem. B*, 2003, **107**, 11690-11699.
28. Alloway, D. M.; Graham, A. L.; Yang, X.; Mudalige, A.; Colorado, R.; Wysocki, V. H.; Pemberton, J. E.; Randall Lee, T.; Wysocki, R. J.; Armstrong, N. R. *J. Phys. Chem. C*, 2009, **113**, 20328-20334.
29. Song, C. K.; White, A. C.; Zeng, L.; Leever, B. J.; Clark, M. D.; Emery, J. D.; Lou, S. J.; Timalsina, A.; Chen, L. X.; Bedzyk, M. J.; Marks, T. J. *ACS Appl. Mater. Interfaces*, 2013, **5**, 9224-9240.
30. Ganzorig, C.; Kwak, K.-J.; Yagi, K.; Fujihira, M. *Appl. Phys. Lett.*, 2001, **79**, 272-274.
31. Paramonov, P. B.; Paniagua, S. A.; Hotchkiss, P. J.; Jones, S. C.; Armstrong, N. R.; Marder, S. R.; Brédas, J.-L. *Chem. Mater.*, 2008, **20**, 5131-5133.
32. Hotchkiss, P. J.; Li, H.; Paramonov, P. B.; Paniagua, S. A.; Jones, S. C.; Armstrong, N. R.; Brédas, J.-L.; Marder, S. R. *Adv. Mater.*, 2009, **21**, 4496-4501.
33. Soreni-Harari, M.; Yaacobi-Gross, N.; Steiner, D.; Aharoni, A.; Banin, U.; Millo, O.; Tessler, N. *Nano Lett.*, 2008, **8**, 678-684.
34. Munro, A. M.; Zacher, B.; Graham, A.; Armstrong, N. R. *ACS Appl. Mater. Interfaces*, 2010, **2**, 863-869.
35. Shalom, M.; Rühle, S.; Hod, I.; Yahav, S.; Zaban, A. *J. Am. Chem. Soc.*, 2009, **131**, 9876-9877.
36. Goh, C.; Scully, S. R.; McGehee, M. D. *J. Appl. Phys.*, 2007, **101**, 114503-.
37. Chen, M.; Fu, W.; Shi, M.; Hu, X.; Pan, J.; Ling, J.; Li, H.; Chen, H. *J. Mater. Chem. A*, 2013, **1**, 105-111.
38. M. Ramanathan, I. I. S. M. Kilbey, Q. Ji, J. P. Hill and K. Ariga, *J. Mater. Chem.*, 2012, **22**, 10389-10405.
39. W. Ding, J. Lin, K. Yao, J. W. Mays, M. Ramanathan and K. Hong, *J. Mater. Chem. B*, 2013, **1**, 4212-4216.

40. Deibel, C.; Strobel, T.; Dyakonov, V. *Adv. Mater.*, 2010, **22**, 4097-4111.
41. Ohkita, H.; Cook, S.; Astuti, Y.; Duffy, W.; Tierney, S.; Zhang, W.; Heeney, M.; McCulloch, I.; Nelson, J.; Bradley, D. D. C.; Durrant, J. R. *J. Am. Chem. Soc.*, 2008, **130**, 3030-3042.
42. Bin, Y.; Yongbo, Y.; Pankaj, S.; Shashi, P.; Rafal, K.; Stephen, D.; Alexei, G.; Ravi, S.; Jinsong, H. *Adv. Mater.*, 2012, **24**, 1455-1460.
43. Cowan, S. R.; Roy, A.; Heeger, A. J. *Phys. Rev. B*, 2010, **82**, 245207.
44. Street, R. A.; Schoendorf, M.; Roy, A.; Lee, J. H. *Phys. Rev. B*, 2010, **81**, 205307.
45. Fu, W.-F.; Chen, X.; Yang, X.; Wang, L.; Shi, Y.; Shi, M.; Li, H.-Y.; Jen, A. K. Y.; Chen, J.-W.; Cao, Y.; Chen, H.-Z. *Phys. Chem. Chem. Phys.*, 2013, **15**, 17105-17111.
46. Zhou, Y.; Eck, M.; Veit, C.; Zimmermann, B.; Rauscher, F.; Niyamakom, P.; Yilmaz, S.; Dumsch, I.; Allard, S.; Scherf, U.; Krüger, M. *Sol. Energy Mater. Sol. Cells*, 2011, **95**, 1232-1237.

